

Comparison of Electrogram Organization and Synchronization Indices in Atrial Fibrillation: a Simulation Study

F Simón^{1,3}, A Arenal², P Laguna^{1,3}, JP Martínez^{1,3}

¹Communications Technology Group (GTC), I3A, IIS Aragón, University of Zaragoza, Zaragoza, Spain

²Department of Cardiology, Gregorio Marañón General University Hospital, Madrid, Spain

³CIBER of Bioengineering, Biomaterials and Nanomedicine (CIBER-BBN), Spain

Abstract

In this work, a comparative study of several electrogram (EGM) organization and synchronization indices in atrial fibrillation (AF) has been performed. To do this, a realistic EGM simulator has been designed. In order to see how the indices are affected by noise and local activation time and conduction variability, the signal-to-noise ratio (SNR), the delay between leads and its variability have been modified in a controlled way. With these different signals, several EGM risk indices (based on spectral, cross-covariance, information and wavefront analysis) have been calculated. Results suggest that indices based on spectral and cross-covariance analysis (organization index, spectral coherence and maximum normalized cross-covariance) are more robust than those based on wavefront or cross-information in quantifying the organization, synchronization and delay when SNR is reduced.

1. Introduction

Atrial fibrillation (AF) is a type of cardiac arrhythmia due to electrical re-entry in the atria. As a result, there is no uniform atrial contraction, inadequate blood pumping from atrium to ventricle and erratic and fast ventricular rate. It is the most common arrhythmia [1] and is a frequent cause of cardiac embolism and heart failure decompensation.

To reverse AF to sinus rhythm, electrical and pharmacological cardioversion are used. If this does not work, radiofrequency ablation is performed (to burn atrial zones in order to avoid electrical re-entry by means of cardiac catheterization). Ablation methods were proposed and are currently under investigation [2]. Electrogram signals (EGM) were obtained by locating electrodes on the cardiac walls. EGM signals analysis provides information about local electrical activity. This information was analyzed and several indices were proposed in the literature to quantify organization, synchronization and delay between different EGM leads.

The main goal of this work is to perform a comparative study of EGM organization and synchronization indices in AF. For that purpose, an EGM simulator based on real EGM has been designed to study the effect of noise and variability in the activation delays.

2. Methods

2.1. Simulation setup

We selected a 2-min real EGM lead recorded during AF at a sampling frequency of 977 Hz as the basis for the simulations, and generated delayed versions by shifting the record with specific delays ($\Delta \in \{10;85\}$ ms, every 10ms). Activation times of the original EGM were automatically detected with the method explained later. Additional variability in the activation times is simulated by advancing or delaying each activation with independent random shifts with zero mean and standard deviations σ (1, 2, 5, 8, 10, 15, 20, 25 and 30 ms, as well 0 ms, no additional variability). This allows us to gradually simulate disorganization in single EGM, and loss in the synchronization between pairs of EGMs. Finally, Gaussian noise is added to the simulated EGMs, so that a given signal-to-noise ratio (SNR) is obtained. Simulated SNR ranged from -10dB to 30dB, every 5dB. For each combination of values, 50 realizations were simulated.

2.2. EGM preprocessing

Filtering: First, we applied a band-pass linear filter (40-250 Hz passband) to attenuate both slow deflections and high frequency noise. The filtered signal was rectified (which makes most energy go to low frequencies), and finally, a linear low-pass filter (with 20 Hz cut-off frequency) was applied. After this preprocessing, the filtered signal shows a positive pulse for each activation [3–5].

Activation detection: it is based on finding positive peaks in the filtered signal, greater than an adaptive threshold proportional to the average amplitude of the last activations[4]. To strengthen the activation detection process, some conditions were added to the actualization threshold rule: 1) the threshold is reduced by 30% after every 200ms without detected activations; 2) a 50ms safety margin or refractory period is defined after an activation detection, to avoid multiple detections of the same activation; 3) if the interval between two detected activations is longer than 1.25 times the inverse of the dominant frequency (section 2.4), a new search is performed reducing the threshold by 30%.

2.3. Wavefront detection

After detecting activations in each EGM lead, we want to group those belonging to the same wavefront [5]. For this purpose we used the method proposed in [4], assuming that two activations from adjacent leads belong to the same wavefront if they are closer than 90 ms. As a result, for each pair of EGM leads, i, j , we obtain a delay vector $\delta_{i,j}$ whose components are the delays between activations of both leads belonging to the same wavefront.

2.4. Organization/synchronization indices

Spectral analysis: The Welch averaged periodogram, with a 2-second Hanning window and 50% overlap, was used to estimate the power spectral density (PSD) of each 10-s segment of the preprocessed signal. The dominant frequency, f^D , is defined as the frequency of maximum PSD between $f_m = 1.5$ and $f_M = 20$ Hz [6]. The ratio of the area under the estimation of PSD in $f^D \pm 0.75$ Hz and the total area from f_m to f_M , is called regularity index, I^R [7]. The organization index, I^O [3], is defined in a similar way, but including also in the numerator the areas under the harmonic frequencies of f^D ($2f^D \pm 0.75$ Hz, $3f^D \pm 0.75$ Hz...) which are within f_m to f_M . Both I^R and I^O quantify how organized are the activations within an EGM lead.

To study the synchronization between leads, we previously proposed to use the averaged coherence index, Γ , defined as the averaged spectral coherence modulus in $f_{i,j}^D \pm 0.75$ Hz, where $f_{i,j}^D$ is the dominant frequency of the cross-spectrum between i and j leads. Γ has a value near 1 if dominant periodicities of both leads are synchronized.

Cross-covariance analysis: The maximum normalized cross-covariance $\rho_{i,j}$ between each pair of preprocessed leads, $y_i(n)$ and $y_j(n)$, was obtained as well as the lag $\tau_{i,j}$ where that maximum appears (which are indices of synchronization and delay between both leads, respectively).

$$\tau_{i,j} = \arg \max_k |c_{i,j}(k)|, \quad (1)$$

$$\rho_{i,j} = \frac{|c_{i,j}(k)|}{\sqrt{c_i(0) \cdot c_j(0)}} \Big|_{k=\tau_{i,j}} \quad (2)$$

where $c_{i,j}(k)$ denotes the cross-covariance function and $c_i(k)$ the autocovariance function.

Information analysis: we also studied indices based on mutual information (MI), used to describe flow of information in other biomedical signals [8]. First, we applied quantization to the preprocessed signal, $y_i(n)$, obtaining $y_i^B(n)$ with $B=8$ levels or bins ($b=1 \dots B$). The probability distribution of each lead, and the joint distribution for a pair of leads is estimated as the histogram and joint histogram for each 10-s segment. For the estimated discrete probability distribution $p_{y_i}(b)$, Shannon's information is defined as

$$H_{y_i} = - \sum_{b=1}^B p_{y_i}(b) \cdot \log_2 p_{y_i}(b) \quad (3)$$

and a similar equation define Shannon's mutual information $H_{y_i y_j}$. Then, the MI of two EGM signals is given by

$$I_{y_i y_j} = H_{y_i} + H_{y_j} - H_{y_i y_j} \quad (4)$$

The mutual information function (MIF) is obtained by computing the MI of the two signals with different delays. The maximum of the normalized MIF [8], $\rho_{i,j}^I$, and the lag $\tau_{i,j}^I$ where the maximum appears were obtained as indices of synchronization and delay, respectively.

Wavefront analysis: After the wavefront detection described in Section 2.3, the consistency of the activation delays was measured by calculating the interquartile range of the delays in the $\delta_{i,j}$ vector. If two EGM leads are well synchronized, the $C_{i,j}^{IQR}$ value should be small. We also calculate a normalized consistency index ($CE_{i,j}$) with values between 0 and 1, based on the Shannon entropy of the delays in the $\delta_{i,j}$ vector [4]. Besides, the median delay $\mu_{i,j}$ (ie, the median of the delays in $\delta_{i,j}$) is also obtained.

In summary: All indices are computed for every 10-second window of the signal. The average value of the indices in each 2-minute realization is computed. The scheme of the processing performed is shown in Fig.1.

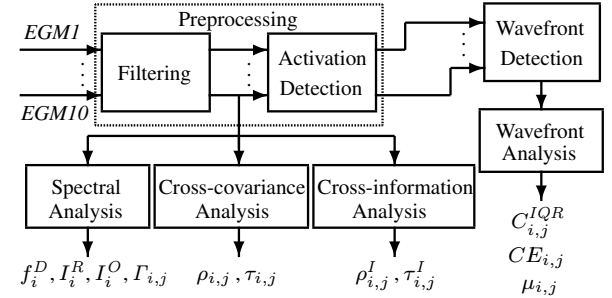


Figure 1. Processing scheme.

3. Results

Mean \pm standard deviation ($m \pm \sigma$) of each index in the simulated realizations are presented, including all possible delays $\Delta \in \{10,85\}$ ms. Fig.2 shows $m \pm \sigma$ of f^D , I^R and I^O for the simulated value of SNR and additional standard deviation σ of the activation times. A similar representation is shown in Fig.3 for the synchronization indices (C^{IQR} , CE , Γ , ρ and ρ^I). Last, Fig.4 shows $m \pm \sigma$ of the errors ϵ_x between the delay indices and the true simulated delays ($\epsilon_x = x - d$, with $x \in \{\mu, \tau, \tau^I\}$ and d the real delays) for the simulated value of SNR and σ of the activation times. In all figures, dotted lines show the trend of the mean index values for $\sigma = 0$ ms and decreasing SNR, while dashed lines show the trend with increasing activation variability for each SNR.

4. Discussion

The simulation setting we have designed allows us to study how the noise and an increased variability in activation delays do affect several well-known and other proposed indices to quantify EGM organization, as well as synchronization and delay between pairs of EGM leads.

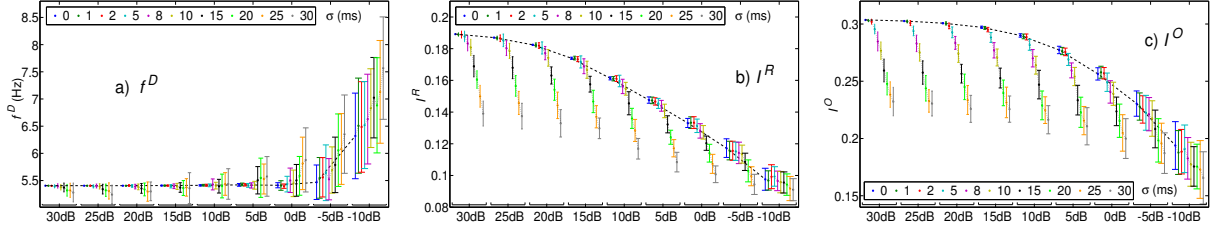


Figure 2. $m \pm \sigma$ values of (a) f^D and organization indices, (b) I^R and (c) I^O .

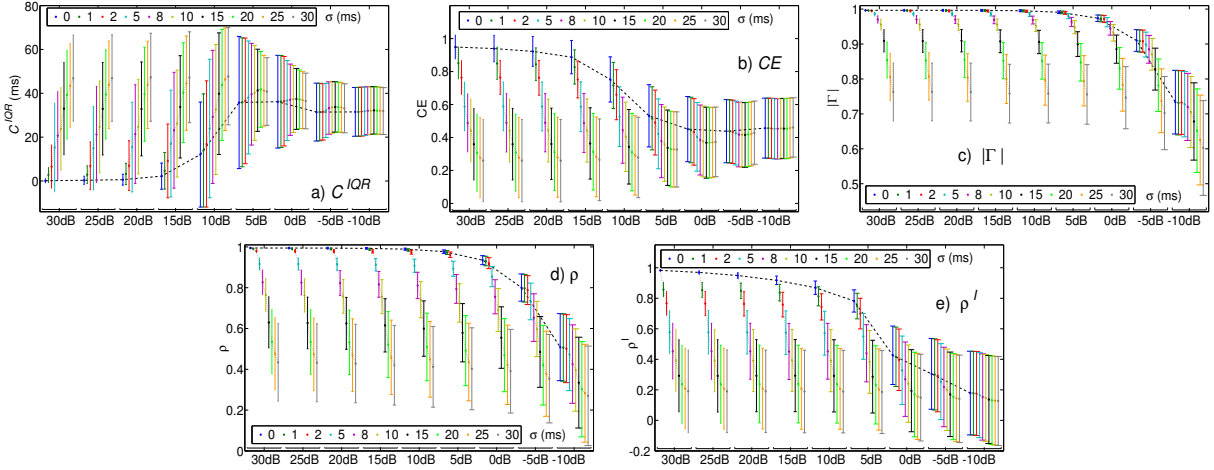


Figure 3. $m \pm \sigma$ values of synchronization indices: (a) C^{IQR} , (b) CE , (c) Γ , (d) ρ , (e) ρ^I .

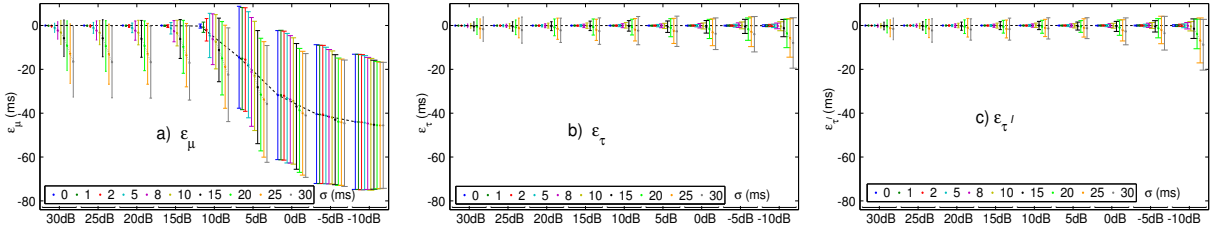


Figure 4. $m \pm \sigma$ values of ϵ_x (differences between the delay indices and the true simulated delays): (a) ϵ_μ , (b) ϵ_τ , (c) ϵ_{τ^I} .

The EGM realizations with an increased value of σ do indeed present a lower organization, and therefore, one would expect decreased organization indices. The same applies for synchronization indices: as the variability applied to each lead is independent, the effect is equivalent to a decrease in the leads' synchronization. The average delay, however, is not changed by the addition of variability in the activation times, and so differences in the delay estimates should be considered as errors.

When noise is added to the EGM, we expect that the quantification of organization, synchronization and delay between leads will be degraded. In this work, we try to assess how indices are degraded by noise, and whether they are able to distinguish differences in organization and synchronization even in the presence of noise.

Dominant frequency: With $\sigma = 0$ ms (no activation variability), Fig.2a shows that the estimated f^D and its variance increase with decreasing SNR value (5.4 ± 0.0 Hz at SNR =

30dB vs 6.3 ± 0.8 Hz at SNR = -10dB). However, the effect is negligible at SNR > 0dB. Increasing the variability of the activation times also increased the variance of the estimated f^D . The effect on the variability led to a slight underestimation of f^D at SNR > 5dB, and a larger overestimation at SNR < -5dB (e.g, at SNR = 25dB, 5.4 ± 0.0 Hz for $\sigma = 0$ ms and 5.2 ± 0.2 Hz for $\sigma = 30$ ms; at SNR = -5dB, 5.5 ± 0.3 Hz for $\sigma = 0$ ms and 6.4 ± 0.7 Hz for $\sigma = 30$ ms).

Organization indices: Fig.2b and 2c show the behavior of I^R and I^O indices for different simulation parameters. As expected, for good SNR, both indices show the maximum organization for $\sigma = 0$ ms and decrease when additional variability is simulated. Adding noise to the signals has the effect of measuring a lower organization index, and also reducing the ability to distinguishing between realizations with different σ . The results show that I^O is more robust than I^R (e.g, at SNR = 5dB and $\sigma = 0$ ms, I^O value is a 91.2% of the value at SNR = 30dB, while I^R is a 78.0%), due to harmonic frequencies that I^O takes into account.

Synchronization indices: Fig.3 shows the effect of the simulation parameters in the synchronization indices studied in this work. As expected, with high SNR, C^{IQR} (Fig.3a) increases and the rest of indices (CE , Γ , ρ and ρ^l , which have a range from 0 to 1) decrease with increasing value of σ (ie, when we simulate a decrease in synchronization between leads). We must note that CE is the “normalized” index presenting a higher variance, even without increased variability. This is due to the fact that CE (and C^{IQR} , which is also based on the estimated wavefront delays) does not behave equally for different simulated conduction delays Δ .

We observe that CE and C^{IQR} (Fig.3a and 3b) experience an important degradation at $SNR \leq 10$ dB, and their values for $SNR \leq 0$ dB do not even change when signals with different values of σ are analyzed, suggesting that the noise is dominating the analysis. The maximum mutual-information index ρ^l (Fig.3e) presents a slight progressive fall from 30dB to 5dB, and exhibits an important degradation at $SNR \leq 0$ dB. The averaged coherence index Γ , and the maximum cross-covariance ρ are much more robust against noise, as the noise does not affect these indices for $SNR > 0$ dB; e.g. at $SNR=30$ dB and $\sigma=0$ ms, CE , Γ , ρ and ρ^l are 0.9 ± 0.1 , 1.0 ± 0.0 , 1.0 ± 0.0 and 1.0 ± 0.0 ; at $SNR=0$ dB and $\sigma=0$ ms are 0.5 ± 0.2 , 1.0 ± 0.0 , 0.9 ± 0.0 and 0.4 ± 0.2 ; at $SNR=15$ dB and $\sigma=5$ ms, are 0.6 ± 0.2 , 1.0 ± 0.0 , 0.9 ± 0.0 and 0.6 ± 0.1 ; at $SNR=15$ dB and $\sigma=25$ ms are 0.3 ± 0.2 , 0.8 ± 0.1 , 0.5 ± 0.2 and 0.2 ± 0.3 .

Delay estimates: The errors for the studied delay estimates (Fig.4) reveal that the median delay μ computed from the wavefront analysis is the less robust. Increasing the variability of the individual activation delays makes μ to underestimate the delay, and increases significantly the estimation variance, and when the noise level is increased, the degradation of μ is important for $SNR \leq 5$ dB (at $SNR=30$ dB, ϵ_μ is 0.0 ± 0.0 ms with $\sigma=0$ ms and -9.2 ± 11.4 ms with $\sigma=20$ ms; at $SNR=0$ dB, is -31.7 ± 29.4 ms with $\sigma=0$ ms and -38.7 ± 28.3 ms with $\sigma=20$ ms). On the contrary, we observe that the estimates based on the maximum cross-covariance and mutual information, τ and τ^l show a much more robust behavior: increasing σ produces a limited underestimation and a slight increase in variance, while the effect of noise is virtually negligible for $SNR > -10$ dB (at $SNR=30$ dB, ϵ_τ and ϵ_{τ^l} are 0.0 ± 0.0 ms with $\sigma=0$ ms and -0.5 ± 3.6 ms and -0.4 ± 3.0 ms with $\sigma=20$ ms; at $SNR=0$ dB, are -0.0 ± 0.1 ms with $\sigma=0$ ms and -1.6 ± 4.4 ms and -1.0 ± 3.5 ms with $\sigma=20$ ms). The results show that τ^l has a RMSE slightly better than τ (3.4 ms vs 3.7 ms), but with large computational load.

5. Conclusions

The results of this simulation study show that indices based on wavefront analysis (C^{IQR} , CE and μ) are much more sensitive to the presence of noise than the rest of

studied indices. These indices strongly depend on the performance of the activation detection stage, and simulation results suggest that the detector we use is very much degraded by noise, at SNR even at 10dB. A more robust detector must be used to obtain reliable synchronization and delay indices based on wavefront analysis. This study shows that the most robust indices are those based on spectral estimation and time-domain covariance: I^o to measure organization, the spectral index Γ (averaged coherence) and the time-domain ρ (maximum cross-covariance) to quantify synchronization, and the lag τ with maximum cross-covariance to estimate the conduction delay.

Acknowledgements

Study supported by TEC2010-21703-C03-02 from CICYT and FEDER, DGA through Grupos Consolidados GTC ref:T30 and CIBER-BBN (CIBER of Bioengineering, Biomaterials and Nanomedicine is an initiative of ISCIII).

References

- [1] Heeringa J, van der Kuip DA, Hofman A, Kors JA, van Herpen G, Stricker BH. Prevalence, incidence and lifetime risk of atrial fibrillation: the rotterdam study. In *European heart journal*, volume 27(8). 2006; 949–953.
- [2] Cappato R, Calkins H, Chen SA, Davies W, Iesaka Y, Kalman J, Kim YH, Klein G, Packer D, Skanes A. Worldwide survey on the methods, efficacy, and safety of catheter ablation for human atrial fibrillation. In *Circulation*, volume 111(9). 2005; 1100–1105.
- [3] Everett TH, Kok LC, Vaughn RH, Moorman JR, Haines DE. Frequency domain algorithm for quantifying atrial fibrillation organization to increase defibrillation efficacy. *IEEE Transactions on Bio medical Engineering* 2001;48:969–78.
- [4] Richter U, Stridh M, Husser D, Cannom DS, Bhandari AK, Bollmann A, Sörnmo L. Wavefront detection from intra-atrial recordings. In *CinC*. 2007; 97–100.
- [5] Simón F, Arenal A, Laguna P, Martínez JP. Stability and correlation of electrogram organization and synchronization indices during atrial fibrillation. *CinC* 2009;149–152.
- [6] Ng J, Kadish AH, Goldberger JJ. Effect of electrogram characteristics on the relationship of dominant frequency to atrial activation rate in atrial fibrillation. In *Heart rhythm: the official journal of the Heart Rhythm Society*. 2006; .
- [7] Fischer G, Stuhlinger MC, Nowak CN, Wieser L, Tilg B, Hintringer F. On computing dominant frequency from bipolar intracardiac electrograms. *IEEE Transactions on Bio medical Engineering* 2007;54(1):165–169.
- [8] Hoyer D, Pompe B, Chon KH, Hardraht H, Wicher C, Zwiener U. Mutual information function assesses autonomic information flow of heart rate dynamics at different time scales. In *IEEE Transactions on Biomedical Engineering*, volume 52. April 2005; 584–592.

Address for correspondence:

Fernando Simón Vadillo, fsimon@unizar.es

María de Luna 1, Ada Byron, Lab 2.05, 50018, Zaragoza, Spain